

PCCP

Accepted Manuscript



This is an *Accepted Manuscript*, which has been through the Royal Society of Chemistry peer review process and has been accepted for publication.

Accepted Manuscripts are published online shortly after acceptance, before technical editing, formatting and proof reading. Using this free service, authors can make their results available to the community, in citable form, before we publish the edited article. We will replace this *Accepted Manuscript* with the edited and formatted *Advance Article* as soon as it is available.

You can find more information about *Accepted Manuscripts* in the [Information for Authors](#).

Please note that technical editing may introduce minor changes to the text and/or graphics, which may alter content. The journal's standard [Terms & Conditions](#) and the [Ethical guidelines](#) still apply. In no event shall the Royal Society of Chemistry be held responsible for any errors or omissions in this *Accepted Manuscript* or any consequences arising from the use of any information it contains.

A new two-dimensional metal-organic framework with high spin-filtering efficiency

Bikash Mandal and Pranab Sarkar*

Department of Chemistry, Visva-Bharati University, Santiniketan- 731235, India

E-mail: pranab.sarkar@visva-bharati.ac.in

Abstract

Here we propose a family of two-dimensional organometallic lattices based on first principle calculations. The proposed lattice is designed by assembling molecular building blocks of naphthalene molecule functionalized by -NH groups and transition metals which are surrounded by four -NH moiety, creating a square planar geometry. The predicted organometallic lattices (with Fe, Cr and Co) are shown to exhibit half metallicity and therefore this class of materials has great promise for spintronics application.

*To whom correspondence should be addressed

1 Introduction

In the recent years, two-dimensional(2-D) materials have attracted immense interest due to their unique physical and chemical properties and potential applications in future electronics. Graphene¹ is one of the most promising 2-D materials for future generation electronics because of its attractive properties such as quantum hall effect, high thermal conductivity, remarkable electron mobility etc. However, application of graphene is restricted in many cases, mainly in semiconductor based devices, because of its zero band gap. The different ways to increase the band gap are the dimensional reduction of graphene to ribbon and quantum dot and chemical functionalization of the graphene but electron mobility drastically reduced because of these. Therefore, researchers have dedicated numerous efforts in fabrication of other 2-D materials with intrinsic non-zero band gap and the success is achieved in different forms e.g BN sheet, silicene, germanane, graphyne, graphdiyne, graphitic carbon nitride, MoS₂ sheet, WS₂ sheet and very recently metal-organic crystals.²⁻¹¹ These 2-D materials have wide range of applications such as high on/off ratio in field effect transistors, large rectification ratio in negative differential resistance, huge spin filtering efficiency, topologically insulating behavior etc. and have the potential to be an alternative to graphene.

The metal-organic frameworks (MOFs) consisting of aromatic organic moieties bridged by square-planar metal center have many fascinating properties and focus of current research.^{8,9} One of the main driving forces for this research field is the potential application of MOFs. The MOF possesses high degree of synthetic flexibilities through the choice of different organic ligands and also metal centers. Taking advantage of this one can tune the electrical, optical and magnetic properties of MOFs. The possibility of tuning has lead to a remarkable range of electronic, optical and magnetic properties and the realization of materials with diverse properties. So, this plays a key role to design new MOFs with superior properties as compared to the existing one. The applicability of MOFs ranges from displays, sensors, light emitting diodes, photo-detectors to the recent third generation solar cells.

The magnetic properties of solids is of crucial interest because of its versatile application in many fields. One very important types of magnetic materials that has attracted lot of attention

in the recent past is spintronic materials. A spintronic device uses spin in addition to charge as an information carrier and by virtue of the spin polarized state this spintronic devices has the promise to bring a revolution in information technology. Half-metal¹² is a class of materials, which have the ability to produce 100% spin-polarized current at the Fermi level due to coexistence of metallic eigen states with one spin configuration and semiconducting eigen channels with the other. Half-metallicity has been observed in many materials such as Heusler compounds,¹² metal-DNA complex,¹³ manganese perovskites,¹⁴ transition metal doped magnetic semiconductor,¹⁵ but graphene based materials attract intensive attention due to long spin coherence length in carbon and their compatibility with the maturing technologies.^{16,17} Zig-zag graphene nanoribbons show half-metallic properties under external electric field or if their edges are modified by appropriate functional groups and because of selective doping¹⁸⁻²¹ The metal-organic frameworks consisting of aromatic organic moieties bridged by square-planar metal ions have many fascinating properties and may be a good candidate to explore those to find out spintronic behaviour.^{9,22-27} There are recent reports on developing porous molecular magnets with different kind of MOF based on first-row transition metals.²⁸⁻³¹ Liu and his co-workers^{5,32,33} have proposed a new hexagonal lattice by assembling a molecular building blocks of triphenyl-transition metal compounds and this exhibits half-metallic behaviour and quantum anomalous Hall effect.

Although the vast majority of MOFs are insulators there are now few recent reports on the synthesis of 2-D metal-organic networks with non-zero band gaps and with good electrical conductivity achieved through full charge delocalization. In a very recent article, Sheberla et al. have synthesized a 2-D semiconducting metal-organic graphene analogue bis(dithiolene) and $Ni_3(HITP)_2$ (HITP = 2,3,6,7,10,11-hexamino triphenylene) which show high electrical conductivity.³⁴ Kambe et al. have synthesized a π -conjugated 2-d nanosheet comprising planar nickel bis(dithiolene) complexes.⁷

Inspired by these innovative experimental studies we here performed a first principle based study to predict a new family of organometallic lattices. The building block of the proposed 2-D lattice is composed of naphthalene molecule functionalized by eight amine groups and transition

metals which are surrounded by four -NH moiety, creating a square planar geometry. Our motivation is to see whether our proposed 2-D crystal can show any interesting material properties with exotic electronic states and may find potential application in the spintronic devices.

2 Computational Method

All first-principles calculations were performed by using density-functional theory (DFT) as implemented in Siesta³⁵ package. We have considered norm-conservative Troullier-Martins pseudopotentials³⁶ and double- ζ plus polarization (DZP) basis set for representing core and valence electrons, respectively. The generalized gradient approximation (GGA) in the Perdew-Burke-Ernzerhof³⁷ (PBE) form is applied to account for electron-electron interactions. The conjugate gradient method is used to relax all the atoms until the maximum force becomes less than 0.01 eV/Å for both primitive unit cells as well as supercells. A real space mesh cutoff of 300 Ry is used throughout the entire calculation and the electronic temperature is set to 300 K. The k-point sampling for unit cells and (4 × 4) supercells were performed with a 8 × 8 × 1 and 2 × 2 × 1 Monkhorst-Pack grid, respectively.

The spin transport properties are simulated by using TranSIESTA module within SIESTA package, which is based on the combination of density functional theory and non-equilibrium Green's function (NEGF).³⁸ We have used similar basis, exchange-correlation functional and convergence criteria as our first-principles calculation. In the NEGF self-consistent loop, the charge density was integrated over 400 energy points along the semicircle in the complex plane. The spin polarized current is calculated with the help of Landauer-Buttiker formula, which can be expressed as:

$$I_{\uparrow(\downarrow)}(V_b) = \frac{e}{h} \int_{\mu_L}^{\mu_R} T_{\uparrow(\downarrow)}(E, V_b) [f_L(E - \mu_L) - f_R(E - \mu_R)] dE \quad (1)$$

where $T_{\uparrow(\downarrow)}$ is the spin-resolved transmission function, $f_{L(R)}$ is the Fermi-Dirac distribution function for the left (right) electrode with electrochemical potential $\mu_{L(R)}$ so that $eV_b = \mu_L - \mu_R$.

3 Results and Discussion

First, we examine the optimized crystal structure of proposed systems. The optimized structure is shown in Figure 1. The rectangular lattices consist of a naphthalene skeleton, whose all hydrogen atoms are replaced by amine groups and two transition metal atoms, which are bridged between adjacent unit cells to create an infinite 2-D sheet. Due to dsp^2 hybridization of metal, square planar geometry is observed surrounding the metal, which is further responsible for planarity of the crystal. For searching new exciting properties, we have designed different crystals using various transition metals, (Cr, Mn, Fe, Co) with different optimum lattice parameters, which are tabulated in Table-1. The optimized lattice constants in X and Y direction respectively are 10.59 Å and 8.53 Å for Cr, 10.44 Å and 8.40 Å for Mn, 10.31 Å and 8.29 Å for Fe, and finally 10.22 Å, 8.23 Å for Co. The C-N bonds, parallel to principal axis of naphthalene molecule, are slightly smaller in length relative to others and the nitrogen atoms of these bonds are slightly closer to the transition metals(M) as compared to remaining M-N bonds.

The stability and plausibility of formation of these crystals can be understood by the formation energy, which is defined as

$$E_f = (E_{tot(sheet)} - m\mu_M - n\mu_N - p\mu_C - q\mu_H)/N$$

where $E_{tot(sheet)}$ is the total energy of the sheet and μ_M , μ_N , μ_C and μ_H , respectively are chemical potential of the metal (calculated from their respective bulk structures), nitrogen (evaluated from nitrogen molecule), carbon (determined from graphene monolayer) and hydrogen atoms (calculated from hydrogen molecule). m, n, p and q count number of metal, nitrogen, carbon and hydrogen atoms respectively and N is total number of atoms in the sheet. The formation energies of these crystals are tabulated in Table-1, from which it is obvious that the fabrication of these lattices is exothermic i.e energetically favorable process, which is very exciting as successful synthesis of these 2-D sheet may open a new direction in materials world and technology.

In order to explore the magnetic coupling pattern between local magnetic moments, we have considered a large-size (2x2) supercell. The geometry of such supercell has been relaxed, starting from two different spin ordering. For the first one, the local magnetic moments are aligned

in ferromagnetic (FM) way and for the other the local magnetic moments are aligned in antiferromagnetic (AFM) way. Our results revealed that FM state is energetically more favorable than AFM state by 7.26 and 70.36 meV, respectively for Cr, Mn with corresponding magnetic moments 24.08 and 28.30 μ_B , while the reverse alignment is more preferable for Fe and Co by 146.01 and 190.27 meV, respectively, without any magnetic moment. Following the analysis of Hu et al.³³ we have tried to understand the calculated magnetic moment of different systems. Basically, the transition metal of all the studied systems are sp^2d hybridized and the structure is square planar. In the presence of local crystal field d orbitals of the transition metal is splitted and the ordering is $d_{yz} = d_{xz} < d_z^2 < d_{xy} < d_{x^2-y^2}$. To meet sp^2d hybridization the number of unpaired electrons in Cr, Mn, Fe and Co should be 4,3,2,1 respectively. The magnetic moment (Table-1) of each Cr is close to 4 (in consistent with the number of unpaired electrons) while the magnetic moments for each Mn, Fe and Co in the lattices are larger as compared to the number of unpaired electrons. To understand this we have analyzed the extent of charge transfer and the larger value is due to the metal to ligand charge transfer and this is maximum in Mn based lattices among the studied systems. So, magnetic coupling between local magnetic moments can be tuned by varying the transition metals and this can open new window in nano-electronics and technology. The further evidence of FM and AFM alignment will be clear from the magnetic charge density which will be discussed later. In this context it is to be noted that planarity of the crystals are well preserved in the supercell for both FM and AFM alignment.

Having studied the magnetic ground state, we are now interested to ascertain the electronic structures of these crystals. Figure 2 represents the spin-resolved band structure of (2x2) supercells containing different transition metals. It is evident that for supercells containing Cr, Fe and Co, valence and conduction bands of up spin channel (blue) are merged, while down spin state (red) possess a certain gap at Γ point, (about 0.80 eV for Cr, 0.79 eV for Fe and 0.39 eV for Co) showing dominance of up spin in charge transport and hence these 2-D organometallic lattices are half-metallic in nature. The situation is different for Mn containing supercell: valence and conduction bands of both spin configuration are overlapped, indicating metallic behavior of the

crystal. It is here worth mentioning that electronic properties of materials specially involving with transition metals may change because of the spin-orbit coupling (SOC). For example Wang et al.^{5,32} in their study found triphenylMn lattice is spin-gapless semiconductor without SOC but it becomes spin semiconductor in presence of SOC. But we believe that there will not be much change in the electronic structure as because the band around the Fermi level are merged. Though Dirac-like crossing points are found in Fe and Co-based systems, but bands around the Fermi level are overlapped within reciprocal space region X- Γ . The band structure of Fe and Co containing lattices show that there is only one spin component around the Fermi level in contrary to the general observation that AFM state is spin-degenerate around the Fermi level. This is presumably due to the spontaneous magnetization induced by the transition metals breaks the time-reversal symmetry and splits the degenerated spin up and spin down bands.³⁹

It is very interesting to note that many bands of both spin alignment for all crystals, got degenerated within a certain zone, M to X in band structure. To investigate the reason of band merging, we have considered two bands of up spin channel of Fe containing crystal, b_1 , b_2 which are merged within M to X and contribution of orbitals for these two wave-functions were evaluated at two different k-points, Γ (at which they are non-degenerate) and M (at which they are degenerate). Analysis of orbital contributions for those two eigen states reveal that p_z orbitals of C, N and d_{xz} , d_{yz} orbitals of Fe are responsible for band merging for these two wave-functions.

Linear dispersion for both spin channels of studied supercells is dominant, within a certain region, mainly Γ to X. Therefore, Dirac-like crossing points have been observed at M point, above and below the Fermi level: at 0.24, -0.099, -0.84 eV for Cr, -0.73 eV for Mn, 0.17, -0.25 eV for Fe and 0.17, -0.28 eV for Co for their up spin state, whereas at -0.14, -0.66 eV for Cr, 0.13, -0.81 eV for Mn, 0.76, -0.58 eV for Fe and 0.40, -0.57 eV for Co for their down spin channel. Dirac-like crossing points have also been observed for up spin state even at the Fermi level for Fe and Co containing lattices, within the region Γ to M. So, there is a possibility of finding Dirac-like fermions in Fe and Co containing crystals at normal condition. It is generally believed that the presence of Dirac bands in graphene is closely related to its hexagonal honeycomb structures and thus are very

common in hexagonal lattices. But interestingly we found Dirac bands in square lattices. By doing theoretical analysis Huang et al.³⁹ and Liu et al.⁴⁰ have shown that square lattices can also have Dirac-like cone dispersions. This dispersion is a consequence of accidental degeneracy. Liu et al.⁴⁰ have shown that although conventional Dirac cones and linear dispersion as those found in graphene are prohibited at M and Γ points in systems possessing full square symmetries however, the high symmetry points X and X' are degenerate and one may have Dirac cones at these points or close to these points. Our systems show the Dirac cones near these high symmetry points. Another feasibility of Dirac-like fermions arises by moving the Fermi level either by doping or by applying an external electric field for all crystals we studied. A very close inspection of the band structure reveals that bands around the Fermi level for up spin channel of Mn, Fe, Co containing lattices is flat within the region M to X. This suggests that movement of electrons with up spin alignment near the Fermi surface is anisotropic i.e motion of up spin electrons along M to X in reciprocal space is more difficult than in other directions. In this context, it is to be noted that dispersion of bands for Fe and Co containing crystals are almost identical around the Fermi level, which suggests that nature of these bands are similar.

To make a concrete conclusion on the origin of half-metallicity, we have plotted orbital resolved spin-polarized density of states of the elements, C, N and Fe, involved in Fe containing (2x2) supercell, in Figure 3. The figure shows that p_z orbitals of C, N and d_{xz} orbital of Fe contribute at the Fermi level in the up spin channel and obviously the half-metallicity is due to these orbitals. The location of these orbitals in energy space suggests that a delocalized π interaction is established throughout the whole sheet through p_z orbitals of C, N and d_{xz} orbital of Fe and thus the non-bonding electrons of nitrogen are delocalized over whole sheet. The figure also reflects significant contribution of p_z orbitals of C, N and d_{yz} orbital of Fe in singly occupied valence band top (SOVBT) and singly unoccupied conduction band minimum (SUCBM) in down spin channel. The nature of contributing orbitals in SOVBT and SUCBM indicates that these two bands are also π type in nature. The type of participating atomic orbitals and their contribution around the Fermi level for Co containing supercell is almost identical with that of Fe containing one. As we have

stated earlier that the nature of bands of Fe and Co containing supercells are similar around the Fermi level, is now confirmed. However, for the 2-D sheet with Cr the reason for half-metallicity is little bit different. The half-metallic behaviour of Cr containing supercell is mainly due to p_z orbitals of C, N and a negligible contribution comes from d_{xz} orbital of Cr. The spin-polarized density of states of Cr containing supercell reveals that net magnetic moment is mainly attributed to d orbitals of the transition metal. Unlike Fe and Co containing crystals, d_{xz} orbital of Cr participates (though contribution is very small) in the formation of SOVBT and SUCBM in down spin channel, with p_z orbital of C and N. Though, these two states are also π type in nature, but their corresponding wave-functions are totally different from that of Fe and Co containing supercells. Thus, for our system, nature of frontier states can be controlled by varying the metal atom and hence the possibility of finding new exciting properties may arise.

To further depict the magnetic coupling between local magnetic moments, we have plotted magnetic charge density, which is defined as charge density difference between up and down spin channels, in Figure 4 for Fe and Cr containing supercells. From the figure it is obvious that for Fe containing crystal, each and every transition metal encompassed by inverse spin on the neighboring transition metals i.e they are antiferromagnetically coupled. From the another point of view, if one move along the diagonal of the supercell then antiferromagnetic alignment between successive transition metals can easily be observed. Actually, total number of transition metals having up spin state is exactly equal to that with net down spin state and as magnitude of local magnetic moments on each and every transition metal is same, net contribution to the overall magnetic moment of the supercell is nil. The situation is same for C and N atoms in the crystal. Therefore, net magnetic moment of the supercell vanishes. The shape of the isosurface on the transition metals indicates significant contribution of d_{z^2} orbital for the generation of local magnetic moment on the transition metals. Analysis of charge density reveals that maximum contribution comes from d_{yz} orbital and d_{xz} orbital also significantly contributes to the local magnetic moment. The situation is totally different for Cr containing supercell: local magnetic moments on the transition metals are all in up spin state i.e they are ferromagnetically coupled and if we neglect few carbon atoms,

which make negligible contribution to the up spin state, then local magnetic moments on nitrogen and carbon atoms are ferromagnetically coupled, but they are in down spin state. However, total magnetic moment for up spin state is much higher than net down spin moment, which results overall magnetic moment of the supercell. The shape of isosurfaces for Cr containing supercell suggests that $d_{x^2-y^2}$ and d_{z^2} orbitals significantly contribute to the local magnetic moment on the transition metals. The charge density analysis exposes that an important contribution comes from d_{yz} and d_{xz} orbitals.

Having detailed information about the magnetic ground state and electronic structure, we have now studied the spintronics^{41,42} properties considering the ground state spin-polarization. A two-probe system, consists of a finite central scattering region (SR) which is confined between semi-infinite left and right electrodes (LE and RE), is considered for transport calculation. The periodic boundary conditions are imposed on the plane normal to the direction of transmission. As the electronic structure Cr, Fe and Co based lattices confirms the half-metallic behaviour, so high spin-filtering efficiency is expected. Therefore, we have studied the transport properties of these systems and their spin-polarized currents (as a function of bias) are depicted in Figure 5. The figure reveals that current for up spin state is much higher than that of down spin state, except for Cr based lattice within a certain bias region (0.4-0.7 V). On the other hand, no significant change has been observed for current associated with the down spin state, over the entire range of bias, which implies the potential of these systems as spin filtering devices. The negative differential resistance (NDR) behavior of up spin state of all the studied systems is distinct in particular bias region. One can understand this NDR behaviour of different lattices from the corresponding band structures. From the band structure of Fe and Co based lattices [Fig. 2 (c) and (d)] we found that there is very low density of states or even a gap (for up spin) in the energy range 0.65 to 0.95 eV and 0.60-0.90 eV respectively and in case of Cr-based lattices Fig. 2(a)] the number of current carrying states of up spin channel decreases around 0.25 eV. The NDR behaviours are observed in the above mentioned energy range of the different systems.

To quantify the extent of spin-resolved current, we have defined the spin-filtering efficiency

(SFE) as:

$$SFE = \frac{I_{\uparrow} - I_{\downarrow}}{I_{\uparrow} + I_{\downarrow}} \times 100 \quad (2)$$

where I_{\uparrow} , I_{\downarrow} are up and down spin current, respectively. As I_{\uparrow} and I_{\downarrow} change with applied bias, so SFE is calculated at different bias and plotted against bias voltage and is shown in Figure 5(lower panel). The variation of SFE is totally symmetric about the zero bias and remarkably it attains the maximum value 100 % within certain bias voltage for all three lattices. Although all the structures show almost 100 % efficiencies however we can compare the efficiencies of different lattices from the range of bias voltage through which it remains 100 %. Hence, to compare relative spin-filtering ability we have calculated the ratio $I_{\uparrow}/I_{\downarrow}$ and plotted in the inset of fig. 5. Obviously, greater the value of the ratio, higher will be spin-filtering ability. The inset reveals that the maximum value of the ratio is almost same for all the lattices as the order of maximum up spin current and minimum down spin current is same for all the systems. However, Fe-based lattice is best among the studied systems as it maintains a constant value of $I_{\uparrow}/I_{\downarrow}$ within a large bias region, -0.9 to 0.9 V, while the remaining two possess a fixed value within a narrow range of bias, -0.4 to 0.4 V and after that the ratio starts to fluctuate and the fluctuation for Cr-based crystals towards lower value of $I_{\uparrow}/I_{\downarrow}$ is much higher compared to that for Co-based system. So, we conclude that among the different systems we studied Fe-based lattices are the best spin filtering material followed by Co and Cr-based lattices. The I-V characteristics as well as high spin-filtering efficiency as manifested by the systems, can be illustrated by spin-polarized transmission function of respective systems and is shown in the Figure 6. The figure reveals a strong and wide transmissions across the Fermi level for up spin states, while there is no transmission for down spin states, for all the systems, which further suggests metallic and semiconducting behavior of up and down spin channels, respectively. The transmission function around the Fermi level implies resonant tunneling between the scattering region and the electrodes, and explicitly responsible for generation of current. Therefore, the wide transmission spectra around the Fermi level for up spin channels accounts for almost the maximum value of SFE.

There are other systems as mentioned in the introduction have spin filtering properties and we now make a comparative account on the spin filtering capacities of these systems. The zigzag silicene nanoribbon(ZSiNR)-based two probe system have shown almost 100 % spin filtering efficiencies only at a certain bias voltage but have lower values at other bias voltages.⁴³ Quantum transport calculations demonstrate that the finite MoS_2NRs and WS_2NR have high spin filtering efficiencies of about 90% and 53% respectively at fermi energy.^{44,45} There are many studies on B and/or N doped graphene nanoribbons showing full spin polarized transport but within a small bias voltage range.⁴⁶⁻⁴⁸ For example, Zheng et al.⁴⁶ in their first principle study on B and N doped graphene nanoribbon found a full spin filtering but only in the voltage bias range -0.3V to +0.3V. Zeng et al.⁴⁷ have studied the charge and spin transport of graphene-based heterostructure and showed that these can act as perfect spin filter only around the fermi energy. Manna et al.⁴⁹ have studied the transport properties of BN-fused polycyclic nanoribbons and have showed 100% spin polarization in the bias voltage $\pm 0.25V$ only. Hu et al.³³ have predicted half-metallic behaviour of 2-D hexagonal organometallic framework made of triphenyl-metal molecules. So this 2-D MOF can also serve as spin filter however these authors didn't calculate the spin filtering efficiencies of this MOF. From the discussion presented above we may conclude that spin filtering efficiencies of MOFs we proposed here are comparable and even better than the other existing 2-D spin filter materials.

4 Conclusion

In this work, based on first principle calculation we have proposed a new 2-D metal-organic crystalline framework, composed of substituted naphthalene moiety and transition metal. The value of the formation energy suggests that the synthesis of this type of metal-organic framework is energetically favorable. The ferromagnetic coupling between local magnetic moments give rise to high magnetic moment for Cr and Mn based supercell, while there is no net magnetic moment for Fe and Co containing supercell due to antiferromagnetic coupling. Among the studied systems, Cr,

Fe, Co based crystals are half-metallic in nature and may find useful application in future generation electronics. The possible origin of half-metallicity of the proposed crystals are explored. The proposed 2-D metal-organic crystals with Fe and Cr metals exhibit remarkable 100 % spin-filtering efficiency so these crystals will serve as good building blocks for spintronic devices. The advent of different synthetic methodologies in organometallic chemistry and substrate mediated molecular self-assembly method results in the realization of different metal-organic frameworks involving several metal atoms and variety of molecules. There are many recent reports of successful synthesis of 2-D metal-organic crystalline materials with metal-C, metal-N, C-C and also other organic bonds.^{7,34,50} In the recent past there are many reports of MOFs where naphthalene used as building blocks.⁵¹⁻⁵³ We have a strong belief that with all these advanced level synthetic techniques the synthesis of our proposed 2-D crystalline materials is highly feasible and thus we suggest a new class of materials to facilitate the design of spintronic devices that will complements graphene.

Acknowledgment The financial supports form CSIR, New Delhi [01(2744)/13/EMR-II] and UGC through research grants are gratefully acknowledged. The author (B. M.) is grateful to CSIR, New Delhi, for the award of Senior Research Fellowship (SRF).

References

- (1) K. S. Novoselov, A. K. Geim, S. Morozov, D. Jiang, Y. Zhang, S. Dubonos, I. Grigorieva and A. Firsov, *Science*, 2004, **306**, 666–669.
- (2) M. Xu, T. Liang, M. Shi and H. Chen, *Chem. Rev.*, 2013, **113**, 3766–3798.
- (3) D. MÃussinger, D. Chaudhuri, T. Kudernac, S. Lei, S. De Feyter, J. M. Lupton and S. HÃuger, *J. Am. Chem. Soc.*, 2010, **132**, 1410–1423.
- (4) A. Du, S. Sanvito and S. C. Smith, *Phys. Rev. Lett.*, 2012, **108**, 197207.
- (5) Z. Wang, Z. Liu and F. Liu, *Nature Commun.*, 2013, **4**, 1471.
- (6) F. Shojaei, J. R. Hahn and H. S. Kang, *Chem. Mater.*, 2014, **26**, 2967–2974.
- (7) T. Kambe, R. Sakamoto, K. Hoshiko, K. Takada, M. Miyachi, J.-H. Ryu, S. Sasaki, J. Kim, K. Nakazato, M. Takata and H. Nishihara, *J. Am. Chem. Soc.*, 2013, **135**, 2462–2465.
- (8) H.-C. J. Zhou and S. Kitagawa, *Chem. Soc. Rev.*, 2014, **43**, 5415–5418.
- (9) V. Stavila, A. A. Talin and M. D. Allendorf, *Chem. Soc. Rev.*, 2014, **43**, 5994–6010.
- (10) C. H. Hendon, D. Tiana, T. P. Vaid and A. Walsh, *J. Mater. Chem. C*, 2013, **1**, 95–100.
- (11) L.-M. Yang, E. Ganz, S. Svelle and M. Tilset, *J. Mater. Chem. C*, 2014, **2**, 7111–7125.
- (12) R. De Groot, F. Mueller, P. Van Engen and K. Buschow, *Phys. Rev. Lett.*, 1983, **50**, 2024.
- (13) S. S. Mallajosyula and S. K. Pati, *J. Phys. Chem. B*, 2007, **111**, 13877–13880.
- (14) J.-H. Park, E. Vescovo, H.-J. Kim, C. Kwon, R. Ramesh and T. Venkatesan, *Nature*, 1998, **392**, 794–796.
- (15) J. E. Medvedeva, A. Freeman, X. Cui, C. Stampfl and N. Newman, *Phys. Rev. Lett.*, 2005, **94**, 146602.

- (16) B. Dlubak, M.-B. Martin, C. Deranlot, B. Servet, S. Xavier, R. Mattana, M. Sprinkle, C. Berger, W. A. De Heer, F. Petroff and et. al., *Nature Phys.*, 2012, **8**, 557–561.
- (17) C. Biswas and Y. H. Lee, *Adv. Funct. Mater.*, 2011, **21**, 3806–3826.
- (18) Y.-W. Son, M. L. Cohen and S. G. Louie, *Nature*, 2006, **444**, 347–349.
- (19) E.-j. Kan, Z. Li, J. Yang and J. Hou, *J. Am. Chem. Soc.*, 2008, **130**, 4224–4225.
- (20) E. Cruz-Silva, Z. Barnett, B. G. Sumpter and V. Meunier, *Phys. Rev. B*, 2011, **83**, 155445.
- (21) S. Dutta, A. K. Manna and S. K. Pati, *Phys. Rev. Lett.*, 2009, **102**, 096601.
- (22) A. K. Cheetham and C. N. R. Rao, *Science*, 2007, **318**, 58–59.
- (23) A. K. Cheetham, C. N. R. Rao and R. K. Feller, *Chem. Commun.*, 2006, 4780–4795.
- (24) E. Coronado and G. Minguez Espallargas, *Chem. Soc. Rev.*, 2013, **42**, 1525–1539.
- (25) H. Oikawa, A. Shigematsu, M. Sadakiyo, T. Miyagawa, K. Yoneda, M. Ohba and H. Kitagawa, *J. Am. Chem. Soc.*, 2009, **131**, 13516–13522.
- (26) C. Rao, S. Natarajan and R. Vaidyanathan, *Angew. Chem. Int. Ed.*, 2004, **43**, 1466–1496.
- (27) M. Kurmoo, *Chem. Soc. Rev.*, 2009, **38**, 1353–1379.
- (28) D. MasPOCH, D. Ruiz-Molina, K. WurSt, N. Domingo, M. Cavallini, F. Biscarini, J. Tejada, C. Rovira and J. Veciana, *Nat. Mater.*, 2003, **2**, 190–195.
- (29) N. Roques, D. MasPOCH, I. Imaz, A. Datcu, J.-P. Sutter, C. Rovira and J. Veciana, *Chem. Commun.*, 2008, 3160–3162.
- (30) N. Roques, D. MasPOCH, F. Luis, A. Camon, K. WurSt, A. Datcu, C. Rovira, D. Ruiz-Molina and J. Veciana, *J. Mater. Chem.*, 2008, **18**, 98–108.
- (31) C. Dey, T. Kundu, B. P. Biswal, A. Mallick and R. Banerjee, *Acta Cryst. B*, 2014, **70**, 3–10.

- (32) Z. Wang, Z. Liu and F. Liu, *Phys. rev. lett.*, 2013, **110**, 196801.
- (33) H. Hu, Z. Wang and F. Liu, *Nanoscale Res. Lett.*, 2014, **9**, 690.
- (34) D. Sheberla, L. Sun, M. A. Blood-Forsythe, S. Er, C. R. Wade, C. K. Brozek, A. Aspuru-Guzik and M. DincÄĀ, *J. Am. Chem. Soc.*, 2014, **136**, 8859–8862.
- (35) J. M. Soler, E. Artacho, J. D. Gale, A. Garca, J. Junquera, P. Ordejon and D. Sanchez-Portal, *J. Phys.: Condens. Matter*, 2002, **14**, 2745.
- (36) N. Troullier and J. L. Martins, *Phys. Rev. B*, 1991, **43**, 1993.
- (37) J. P. Perdew, K. Burke and M. Ernzerhof, *Phys. Rev. Lett.*, 1996, **77**, 3865.
- (38) M. Brandbyge, J.-L. Mozos, P. Ordejon, J. Taylor and K. Stokbro, *Phys. Rev. B*, 2002, **65**, 165401.
- (39) X. Huang, Y. Lai, Z. H. Hang, H. Zheng and C. Chan, *Nature mater.*, 2011, **10**, 582–586.
- (40) Z. Liu, J. Wang and J. Li, *Phys. Chem. Chem. Phys.*, 2013, **15**, 18855–18862.
- (41) Y.-S. Liu, X.-F. Wang and F. Chi, *J. Mater. Chem. C*, 2013, **1**, 8046–8051.
- (42) P. Zhao, Q. H. Wu, H. Y. Liu, D. S. Liu and G. Chen, *J. Mater. Chem. C*, 2014, **2**, 6648–6654.
- (43) X. Yang, Y. Liu, J. Feng, X. Wang, C. Zhang and F. Chi, *J. App. Phys.*, 2014, **116**, 124312.
- (44) Z. Wang, H. Li, Z. Liu, Z. Shi, J. Lu, K. Suenaga, S.-K. Joung, T. Okazaki, Z. Gu, J. Zhou, Z. Gao, G. Li, S. Sanvito, E. Wang and S. Iijima, *J. Am. Chem. Soc.*, 2010, **132**, 13840–13847.
- (45) Z. Wang, K. Zhao, H. Li, Z. Liu, Z. Shi, J. Lu, K. Suenaga, S.-K. Joung, T. Okazaki, Z. Jin, Z. Gu, Z. Gao and S. Iijima, *J. Mater. Chem.*, 2011, **21**, 171–180.
- (46) X. Zheng, R. Wang, L. Song, Z. Dai, X. Wang and Z. Zeng, *App. Phys. Lett.*, 2009, **95**, 123109.

- (47) M. Zeng, L. Shen, M. Yang, C. Zhang and Y. Feng, *App. Phys. Lett.*, 2011, **98**, 053101.
- (48) J. Kang, F. Wu and J. Li, *Applied Physics Letters*, 2011, **98**, 083109.
- (49) A. K. Manna and S. K. Pati, *J. Mater. Chem. C*, 2013, **1**, 3439–3447.
- (50) A. J. Clough, J. W. Yoo, M. H. Mecklenburg and S. C. Marinescu, *J. Am. Chem. Soc.*, 2015, **137**, 118–121.
- (51) G. Li and Z. Wang, *J. Phys. Chem. C*, 2013, **117**, 24428–24437.
- (52) B. D. McCarthy, E. R. Hontz, S. R. Yost, T. Van Voorhis and M. Dincal, *J. Phys. Chem. Lett.*, 2013, **4**, 453–458.
- (53) L. Han, L. Qin, L. Xu, Y. Zhou, J. Sun and X. Zou, *Chem. Commun.*, 2013, **49**, 406–408.

Table 1: Optimized lattice constants(lc), formation energies(E_f) and magnetic moment (MM) per (2×2) supercell as well as per transition metal(TM)

Metal	lc(Å)		E_f (eV/atom)	MM/(2×2) cell(μ_b)	MM/TM (μ_b)
	X-dir	Y-dir			
Cr	10.59	8.53	-0.3311	24.076	3.861
Mn	10.44	8.40	-0.4891	28.301	3.9995
Fe	10.31	8.29	-0.2340	0.0	2.647
Co	10.22	8.23	-0.9132	0.0	1.3915

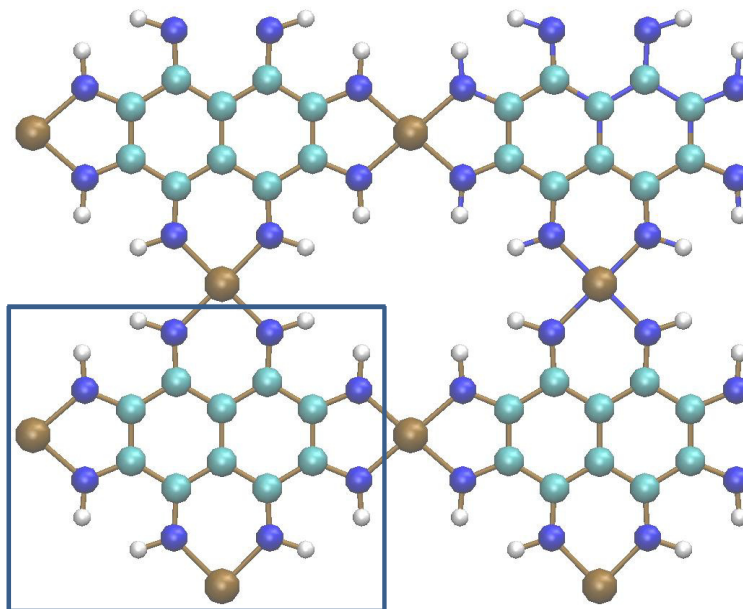


Figure 1: Top view of the 2-D metal-organic superlattice. The rectangular box represent the unit-cell. White, cyan, blue and brown colour spheres respectively are hydrogen, carbon, nitrogen, transition metal.

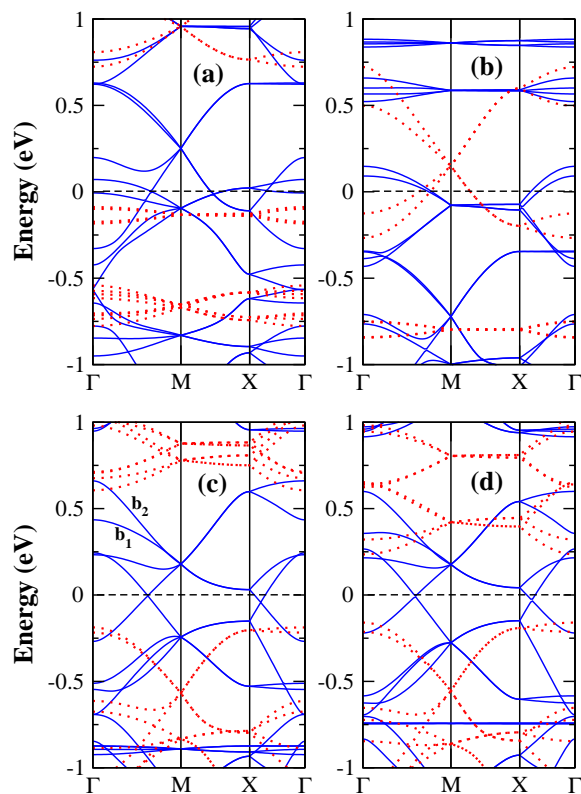


Figure 2: Spin polarized electronic band structure of Cr(a), Mn(b), Fe(c) and Co(d) containing supercells. Solid blue and red dotted lines represent the bands of up and down spin channels, respectively. The black dotted line indicates the Fermi level. Γ , M, X, Γ are the high symmetric k-points of first Brillouin zone.

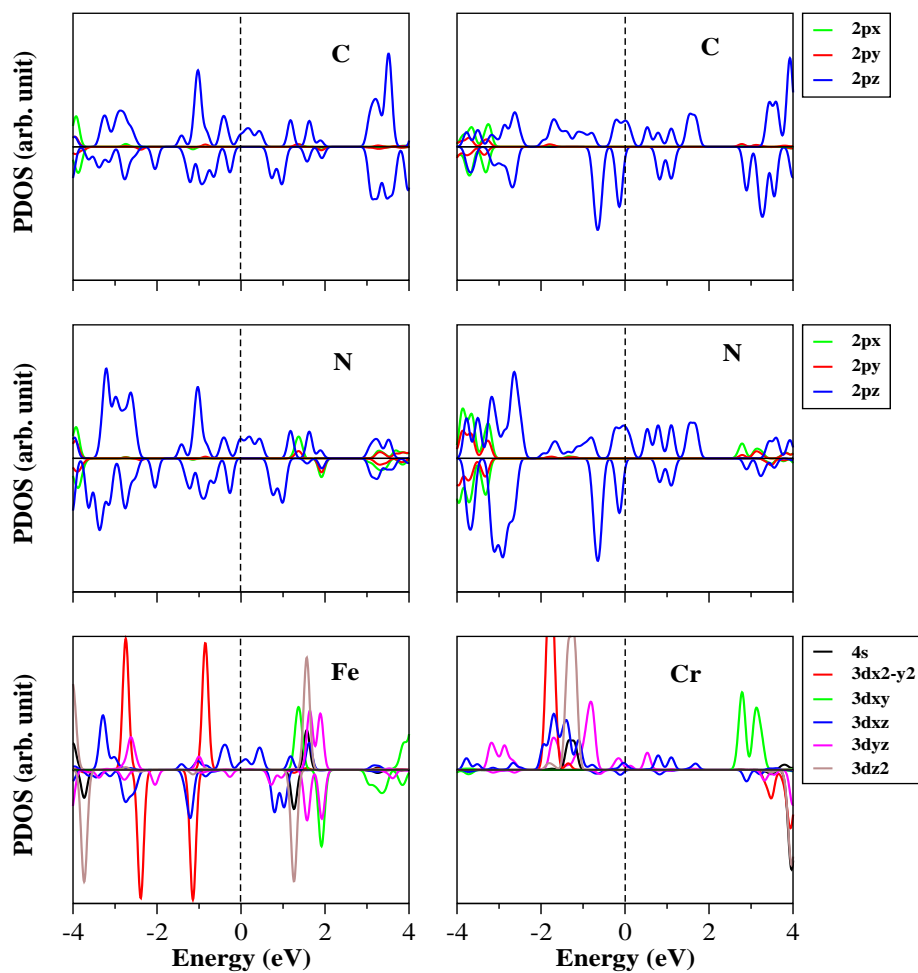


Figure 3: Orbital resolved, spin-polarized projected density of states of Fe containing (left column) and Cr containing (right column) (2x2) supercell, including contribution of all the elements, except hydrogen.

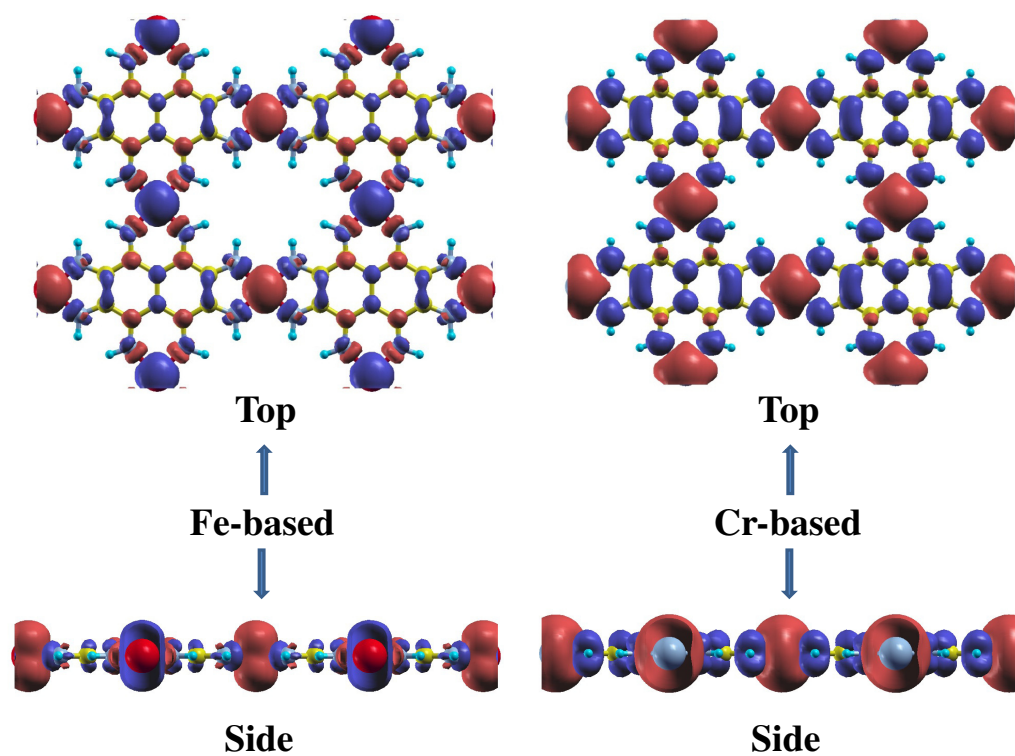


Figure 4: Top and side view of magnetic charge density ($\Delta\rho = \rho_{\uparrow} - \rho_{\downarrow}$) of Fe and Cr based superlattices, in which red and blue isosurfaces show net up and down spin density. Isovalue= 0.002 is used for the charge density plot.

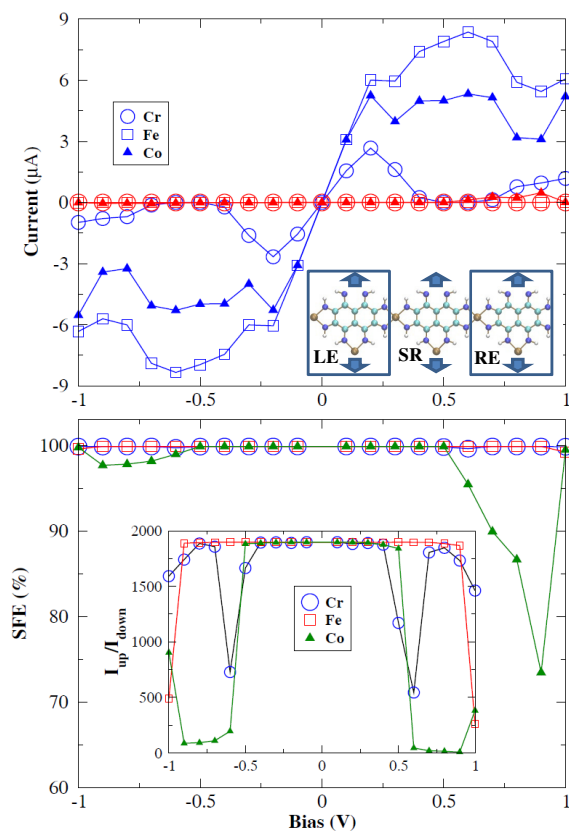


Figure 5: Spin-dependent current-voltage (I-V) characteristics and spin-filtering efficiencies of Cr, Fe and Co based systems. The blue (red) symbols are used to represent up (down) spin current in I-V plot. Circular, square and triangular shapes are used for Cr, Fe and Co based systems, respectively. A schematic representation of the two-probe system is given in the inset of the upper panel. The inset of the lower panel represents the variation of $I_{\uparrow}/I_{\downarrow}$ with bias.

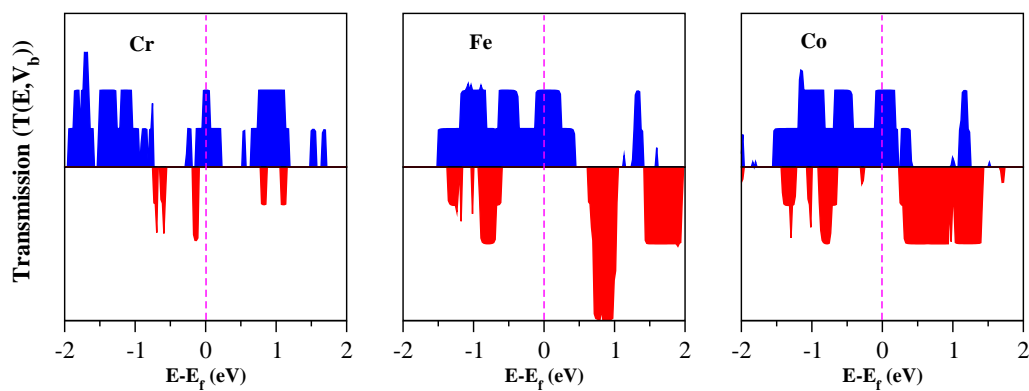


Figure 6: Spin-resolved zero bias transmission function of Cr, Fe and Co based systems. The blue (red) shaded region represent the transmission spectra of up (down) spin channel.